Available online at www.sciencedirect.com

ScienceDirect

IFAC Papers Online CONFERENCE PAPER ARCHIVE

IFAC-PapersOnLine 48-27 (2015) 099–104

Scheduled controller design for systems with two switching sensor configurations: A frequency-domain approach ⋆

S.J.L.M. van Loon * **R. van der Weijst** * **M.F. Heertjes** *,** **W.P.M.H. Heemels** *

* *Mechanical Engineering Department, Eindhoven University of Technology, the Netherlands*
** *ASML Netherlands B.V., Mechatronics System Development, the Netherlands*

Abstract: In this paper, we consider a hybrid system consisting of a motion stage that exhibits, from a control point-of-view, position-dependent dynamics as a result of varying sensor configurations. A scheduled controller design is proposed that is intuitive for control engineers as all individual filters can be obtained using classical frequency-domain loop-shaping techniques thereby connecting to the industrial motion control practice. Moreover, data-based graphical conditions are provided in the frequency-domain under which closed-loop stability can be verified irrespective of how the switching between the controllers occurs in time. The effectiveness of the proposed scheduling technique, as a way to improve both transient and steady-state performance compared to the current state-of-the-art industrial control solution, is demonstrated by means of experiments on a high-precision industrial motion stage.

Keywords: Switched systems, frequency-domain loop-shaping, circle criterion, input-to-state stability, applications.

1. INTRODUCTION

High-precision motion stages, such as positioning devices used in the semi-conductor industry, are subject to ever increasing requirements on stage acceleration (throughput) and positioning accuracy (imaging quality), see, e.g., Butler (2011). As a result, the influence of structural mode deformation in these stages cannot be neglected. The sensor configuration, i.e., the amount and location of the sensors used in the measurement system, yields a specific characterization of these structural dynamics and is therefore essential for control. In many practical situations, the availability of sensors depends on the position of the motion stage as individual sensors can become 'out-of-range' as a result of physical limitations on their operating ranges. As a result, the sensor configuration may vary as a function of the stage position, which essentially makes the stage, from a control point-of-view, a switched system, see Liberzon (2003), or a position-dependent dynamical system. This complicates the overall design significantly, certainly if the design techniques have to connect to the state-of-the-art industrial control context. In fact, an important open problem is the design of control systems for dynamical systems with switching sensor configurations based on, for industry important, tools such as frequency-domain loop-shaping techniques, see, e.g., Steinbuch and Norg (1998). The major advantage of these tools is that they do not necessarily require parametric models but can be based on easy-to-obtain (and accurate) measured frequency response functions (FRFs) characterizing the motion stage dynamics. In the context of switched systems, this forms a tremendous challenge for which many existing approaches do not meet the desired design requirements.

In industry, the problem of position-dependent dynamics is often dealt with by means of robust control design, see, e.g., van de Wal et al. (2002), in which the authors propose an $\mathcal{H}_\infty$-controller for this purpose. Although such an approach meets the desired industrial design requirements, it often results in conservatism because (a) one single linear time-invariant (LTI) controller is active within the whole range of operation, and (b) due to the inherent classical performance trade-offs in LTI feedback control systems, see, e.g., Seron et al. (1997). To overcome these limitations, several (nonlinear) control techniques exist in the literature that can adapt the controller dynamics according to the on-line measured actual position of the system. One such technique is referred to as gain scheduling, see, e.g., Rugh and Shamma (2000); Leith and Leithead (2000). In gain scheduling, the designer typically selects a finite grid of operating points within the whole range of operation. For each of these operating points FRFs are identified, and based on these FRFs, dedicated local LTI controllers are designed which are implemented by interpolation. Although the design and implementation is intuitive for control engineers, no constructive results exist to formally and systematically guarantee stability and performance of the closed-loop gain-scheduled system. Another technique is linear parameter varying (LPV) control, see, e.g., Groot Wassink et al. (2005); Shamma and Athans (1991); Scherer (2001), which leads to parameter-dependent controllers. This technique typically requires a parametric model that describes how the dynamics of a system varies as a function of the position. Compared to our approach, obtaining such parametric models is time-

⋆ This work is supported by the Dutch Technology Foundation (STW) under project "HyperMotion: Hybrid Control for Performance Improvement of Linear Motion Systems" (no. 10953).
**E-mail addresses of the authors: {s.j.l.m.v.loon, r.v.d.weijst, m.f.heertjes, m.heemels}@tue.nl

2405-8963
Peer review under responsibility of International Federation of Automatic Control.
10.1016/j.ifacol.2015.11.159

consuming and often they are still not accurate enough to properly describe the system dynamics. Opposed to gain scheduling, the synthesis of LPV controllers yields a priori guaranteed stability and performance properties of the LPV controlled system. However, contrary to our proposed graphical data-based conditions to verify closed-loop stability, LPV control typically requires solving linear matrix inequalities (LMIs), which from an industrial point-of-view is not easy to adopt as it does not connect to the state-of-the-art industrial design tools. Also many designs for the control of switched systems, see, e.g., Heemels et al. (2010); Liberzon (2003); Deaecto et al. (2011) require accurate parametric models and LMI-based designs that are not so easily embraced by control engineers in industry. As a consequence, there is often a need for design tools for switched systems, such as the class of dynamical systems with position-dependent switching of sensor configurations studied in this paper, that bridge the gap between hybrid systems theory (with formal stability guarantees) and industrial control practice, commonly exploiting frequency-domain design tools and non-parametric models, e.g., measured FRF descriptions of the motion system dynamics.

In this paper, we provide a solution for such an exemplary problem in the context of an industrial motion stage for the lithography industry. In particular, we will adopt a scheduled controller architecture that, based on the on-line measured actual position of the system, switches between dedicated (local) LTI controllers. Moreover, we will show that the overall design of the proposed controller is intuitive for control engineers because, (a) all individual LTI controllers can be designed using classical frequency-domain loop-shaping techniques based on measured FRFs, (b) graphical data-based conditions are provided to verify closed-loop stability under arbitrary switching, and (c) the control architecture allows for implementation of all components in a standard motion control software environment. The practical feasibility of the proposed approach is emphasized by means of a case study on an industrial wafer motion stage, which is also used to demonstrate the potential of the proposed scheduled controller by experimental results, including the improvements it provides with respect to the state-of-the-art industrial control solution.

The remainder of the paper is organized as follows. In Section 2, we will provide the problem formulation and introduce the plant model in the form of a switched system. In Section 3, the proposed control design is introduced and in Section 4 conditions for stability are provided. Finally, experimental results are given in Section 5 and we will end with conclusions in Section 6.

2. PROBLEM FORMULATION AND SYSTEM DESCRIPTION

Section 2.1 introduces the problem as considered in this paper, which is inspired by an industrial wafer stage system. The modeling of such a system is discussed in Section 2.2, and the current industrial solution to deal with this problem is discussed in Section 2.3.

2.1 Introduction to the problem

In this section, we consider a wafer stage system that is schematically depicted in Fig. 1. A wafer stage is a module

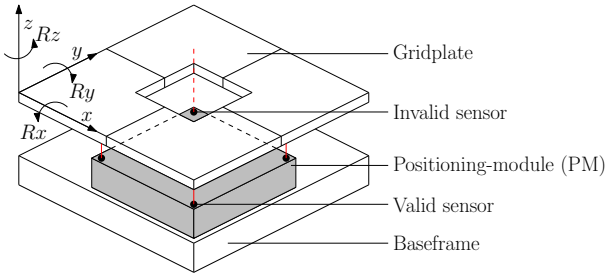

Fig. 1. Schematic representation of a wafer stage.

of a wafer scanner, which is a device used to expose silicon wafers to a light source from an optical column as part of the production process of integrated circuits (ICs), see, e.g., Butler (2011). The positioning-module (PM) supports a wafer and positions this wafer with respect to the light source in both scanning (x, y) and focus (z) direction. The light path enters the stage in negative z-direction at a fixed (x, y)-position (typically the center of the depicted stage). In this respect, the so-called point-of-interest (POI) is defined as the intersection between the light path with the surface of the wafer. This POI is time-varying because the wafer is subject to exposure via a meander-like pattern in the (x, y)-plane.

Our goal is to control the POI such that it tracks the meander-like reference setpoint with a high accuracy. However, the true position of the POI is *not* directly measurable and can only be estimated based on sensor information. The estimation of the POI is called the point-of-control (POC) and will be used for closed-loop servo control. Therefore, the availability of actual sensor information, provided by the measurement system, is crucial for feedback control. For the considered wafer stage, the measurement system consists of four gridplates and four sensors. These sensors are mounted on the PM (indicated by the black dots in Fig. 1) and provide two measurements each (the 2D encoders measure a horizontal and vertical displacement). The square hole surrounded by the gridplates is to enable exposure of the wafer to the light source. However, due to this hole, each of the four sensors can enter an 'out-of-range' state depending on the position of the PM with respect to the gridplates. As a result, the measurement system has five local sensor configurations, namely, one that uses all four sensors, while the other four use a (different) set of three sensors. To make this more precise, we define the range of operation $\Theta \subset \mathbb{R}^2$, i.e., the region in the (x, y)-plane where the wafer stage can operate, and a position vector $\theta(t) \in \Theta$, denoting the actual position of the PM at time $t \in \mathbb{R}_{\geq 0}$. We define regions $\Lambda_i \subseteq \Theta$, $i = 1, 2, \ldots, n$, where each of the sensor configurations is available. Moreover, it holds that $\cup_{i=1}^{n} \Lambda_i = \Theta$, and these regions might be overlapping. In fact, in our case with $n = 5$, they are schematically depicted in Fig. 2(a). In this figure, the subset in which all four sensors are available is denoted by Λ_2, and the subsets in which only three sensors are available are Λ_i, $i \in \{1, 3, 4, 5\}$.

Remark 1. All four sensors are available in region Λ_2, which implies that also the other configurations are available.

Based on the outcome of all available sensors, which each provide two measurements, the displacement of the PM

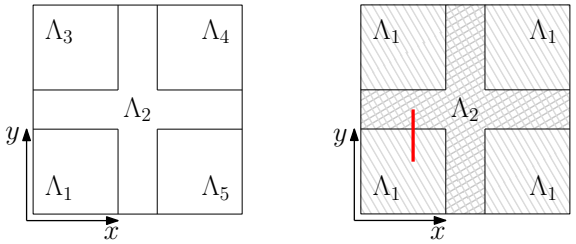

(a) $n = 5$ (b) $n = 2$

Fig. 2. Schematic representation of the subdivision of the range of operation Θ into regions $\Lambda_1, \Lambda_2, \ldots, \Lambda_n$, with (a) $n = 5$, and (b) $n = 2$, in the (x, y)-plane. The red line in Fig. 2(b) represents the location of the setpoint, as considered in Section 5.2, in the (x, y)-plane.

along the orthogonal coordinate system as in Fig. 1, in which the six DOFs of motion are defined, is obtained using coordinate transformations. In this coordinate system, the dynamics along each axis, reconstructed by the measurement system, consists of a rigid body mode and a number of structural modes. In the ideal case, this structural mode behavior should be suppressed by the control system as these structural dynamics complicate the estimation of the exact position of the POI, i.e., when the stage behaves as a rigid body mode we typically have POC=POI, and non-rigid body behavior usually causes POC≠POI. However, due to the limited amount of actuators (six actuators for six modes), feedback control is limited to the control of the rigid body modes only, which is common practice in industrial motion control, see also Butler (2011); van de Wal et al. (2002). To this extent, the measurement system should provide a good six DOF rigid body position estimate as this enables us to achieve an as high as possible controller bandwidth and, as a result, the POC can better track the meander-like reference setpoint. When $\theta \in \Lambda_2$, all four sensors are available and, hence, the measurement system provides eight measurements while only the six rigid body modes are estimated. This is referred to as over-sensing and enables the 'removal' of structural mode behavior in the output, i.e., the appearance of some structural modes are *unobservable* in the output used for controlling the system. When transferring from region Λ_2 to region Λ_i, $i \in \{1, 3, 4, 5\}$, one of the 4 sensors becomes invalid, and as a result, the effect of these structural mode deformations becomes visible in the output, thereby making the rigid body position estimate worse compared to the situation in which all four sensors are available.

2.2 Switched system formulation

In this paper, we focus on controlling the POC in z-direction only, in which the loss of sensor information results in a less accurate rigid body position estimate, as described above. In fact, because the input to the controller is observed by a switched set of sensors depending on the position of the stage in the (x, y)-plane, the z-dynamics exhibits, from *a control (input-output) point-of-view*, position dependent dynamics. As a result, a switched system representation is obtained, which can be modeled by means of different output matrices $C_{\mathcal{P}_i}$, $i = 1, 2, \ldots, 5$. To be precise, the z-dynamics of the motion

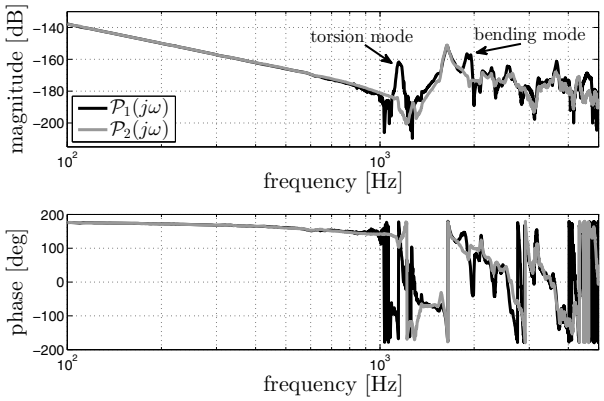

Fig. 3. FRF measurements of the local plants $\mathcal{P}_i(j\omega)$, $\omega \in \mathbb{R}$, $i = 1, 2$.

stage can be represented by a single-input-multi-output (SIMO) switched system of the form

$$\Sigma_{sw} : \begin{cases} \dot{x}_{\mathcal{P}} &= A_{\mathcal{P}} x_{\mathcal{P}} + B_{\mathcal{P}} u_{\mathcal{P}} \\ y_{\mathcal{P}_i} &= \begin{cases} C_{\mathcal{P}_i} x_{\mathcal{P}} & \text{when } \theta \in \Lambda_i \\ \varnothing & \text{when } \theta \notin \Lambda_i, \end{cases} \end{cases} \tag{1}$$

with input $u_{\mathcal{P}} \in \mathbb{R}$, state vector $x_{\mathcal{P}} \in \mathbb{R}^{n_{\mathcal{P}}}$ with $n_{\mathcal{P}}$ the number of states, and output $y_{\mathcal{P}_i} \in \mathbb{R}$, $i = 1, 2, \ldots, 5$, indicating the i-th measured output that is active in its corresponding region Λ_i. When $\theta \notin \Lambda_i$ the output $y_{\mathcal{P}_i}$ is not available, which is indicated by $y_{\mathcal{P}_i} = \varnothing$.

Due to to (1), we can associate 5 local LTI systems to their corresponding regions Λ_i, $i \in \{1, 2, \ldots, 5\}$, which can also be described by the corresponding single-input-single-output (SISO) transfer functions

$$\mathcal{P}_i(s) = \frac{y_{\mathcal{P}_i}(s)}{u_{\mathcal{P}}(s)} \tag{2}$$

with $i = 1, 2, \ldots, 5$ and $s \in \mathbb{C}$. Note that all $\mathcal{P}_i(s)$, $i = 1, 2, \ldots, 5$, share at least two poles at $s = 0$ (because we consider a motion system) and possibly some other dynamics. This allows us to express (2) as

$$\mathcal{P}_i(s) = \mathcal{F}(s)\Delta_{\mathcal{P}_i}(s), \tag{3}$$

in which the shared dynamics are represented by $\mathcal{F}(s)$ and the remaining dynamics by $\Delta_{\mathcal{P}_i}(s)$, $i \in \{1, 2, \ldots, 5\}$. Note that for the systems that we consider, $\Delta_{\mathcal{P}_i}(s)$, $i \in \{1, 2, \ldots, 5\}$ contains stable dynamics only.

To illustrate the possible differences in observed dynamic behavior, consider the regions Λ_i, $i = 1, 2$, in Fig. 2(a), for which FRF measurements of the local plants $\mathcal{P}_i(j\omega)$, $\omega \in \mathbb{R}$, $i = 1, 2$, are given in Fig. 3. Recall that, for $\theta \in \Lambda_2$, some structural modes are unobservable in the output due to over-sensing, and as a result, two structural modes, which appear in $\mathcal{P}_1(j\omega)$, are absent in $\mathcal{P}_2(j\omega)$. To be precise, these modes are the torsion mode at ±1150 Hz, and a bending mode at ±1900 Hz, see Fig. 3.

2.3 Industrial state-of-the-art control design

In industry, control design for systems described by (1) often consists of two steps. First, a single LTI controller $\mathcal{C}(s)$, $s \in \mathbb{C}$, which results in an asymptotically stable closed-loop system for all 5 *individual* local LTI plants $\mathcal{P}_1, \ldots, \mathcal{P}_5$, is designed based on 5 local FRFs using frequency-domain

loop-shaping techniques. Subsequently, in order to use this SISO LTI controller $\mathcal{C}(s)$ with (1), based on the switching outputs $y_{\mathcal{P}_1}, y_{\mathcal{P}_2}, \ldots, y_{\mathcal{P}_5}$, an output scheduling law is introduced, such that from (1) the following SISO LPV system results

$$\dot{x}_{\mathcal{P}} = A_{\mathcal{P}} x_{\mathcal{P}} + B_{\mathcal{P}} u_{\mathcal{P}} \tag{4a}$$

$$y_{\mathcal{P}} = \sum_{i=1}^{n} \phi_i(\theta) C_{\mathcal{P}_i} x_{\mathcal{P}}, \tag{4b}$$

with $y_{\mathcal{P}} \in \mathbb{R}$, and $\phi_i(\theta) \in [0,1]$, $i = 1,2,\ldots,5$, position-dependent output scheduling parameters that satisfy $\sum_{i=1}^{5} \phi_i(\theta) = 1$, and $\phi_i(\theta) = 0$ when $\theta \notin \Lambda_i$ for $i = 1,2,\ldots,5$. Although appealing for industry, this control solution has two significant drawbacks:

(1) There is no a priori guarantee for stability of the closed-loop connection of plant (4) with LTI controller $\mathcal{C}(s)$ for all $\theta(t) \in \Theta$ varying over time;
(2) The control of all local plants with one robust LTI controller $\mathcal{C}(s)$ potentially limits performance.

In the remainder of this paper, we assume that $\mathcal{P}_1$ can be used to describe the plants $\mathcal{P}_i$, $i = 1,3,4,5$ in Fig. 2(a), and hence, $i = 1,2$ in (1) (see Fig. 2(b)). A scheduled controller design for $i = 1,2,\ldots,5$ is a topic for future research, for which the design presented here forms a first important and fundamental step.

Remark 2. In the special case of $i = 1,2$, the regions Λ_i, $i = 1,2$, are described by $\Lambda_1 := \Theta$ and $\Lambda_2 \subset \Theta$, see Remark 1, and depicted schematically in Fig. 2(b). Hence, for $i = 1,2$, one can take $\phi_1(\theta) = 1$ and $\phi_2(\theta) = 0$, $\theta \in \Theta$, (as $y_{\mathcal{P}_1}$ is available for all $\theta \in \Theta$, i.e., $\Lambda_1 = \Theta$) in (4) and design one LTI controller $\mathcal{C}(s)$, $s \in \mathbb{C}$, based on the plant $\mathcal{P}_1(s)$. This would remove the previously mentioned drawback (1), still leaving drawback (2).

3. SCHEDULED CONTROLLER DESIGN

In this section, we present a scheduled controller architecture with the aim to switch between two LTI controllers $\mathcal{C}_i(s)$, $i = 1,2$, based on the actual position $\theta \in \Theta$. The proposed scheduled controller architecture, which is schematically depicted in Fig. 4, results in an effective controller $\mathcal{C}_2(s)$ (designed based on $\mathcal{P}_2(s)$) when $\theta \in \Lambda_2$, and results in $\mathcal{C}_1(s)$ (designed based on $\mathcal{P}_1(s)$) otherwise. Consider Fig. 4, in which $r \in \mathbb{R}$ denotes the reference signal, $d \in \mathbb{R}$ an unknown but bounded disturbance, and Σ_{sw} is given by (1) with $n = 2$, $\Lambda_1 = \Theta$, and $\Lambda_2 \subset \Theta$. The position-dependent scheduling gain is denoted by $\alpha(\theta)$ and can take values in $[0,1]$. Moreover, the (non)availability of $y_{\mathcal{P}_2}$ in (1), and Fig. 4 is modeled via the position-dependent indicator function

$$\beta(\theta) = \begin{cases} 1 & \text{when } \theta \in \Lambda_2 \\ 0 & \text{when } \theta \notin \Lambda_2. \end{cases} \tag{5}$$

The to-be-designed filters $\mathcal{C}_\Delta(s)$ and $\mathcal{C}_2(s)$ in Fig. 4 are both LTI and can be designed using classical frequency domain loop-shaping techniques. The procedure to do so is as follows. The first step in designing these filters is to design dedicated LTI controllers $\mathcal{C}_1(s)$ and $\mathcal{C}_2(s)$, based on measured FRF data of the local plants $\mathcal{P}_1(j\omega)$ and $\mathcal{P}_2(j\omega)$, $\omega \in \mathbb{R}$, respectively. These LTI controllers typically consist of the following linear filters: A PID-type filter, a second-order low pass filter, and a number of notch filters. Because

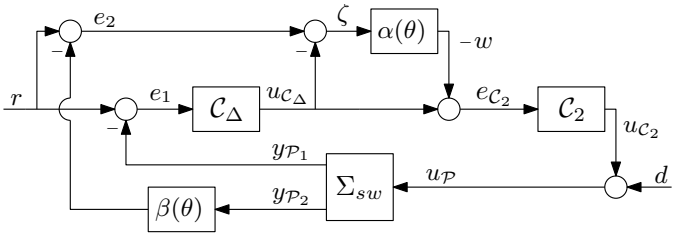

Fig. 4. Schematic representation of the feedback loop with SIMO plant Σ_{sw}, as in (1), and the proposed scheduled controller.

both $\mathcal{C}_i(s)$, $i = 1,2$, contain a PID-type filter, they share at least one pole at $s = 0$ (due to the integrator) and possibly some other dynamics. In step two, the shared dynamics are collected in an LTI filter $\mathcal{H}(s)$ such that

$$\mathcal{C}_i(s) = \mathcal{H}(s)\Delta_{\mathcal{C}_i}(s), \tag{6}$$

in which $\Delta_{\mathcal{C}_i}(s)$, $i = 1,2$, contain the remaining controller dynamics. This allows us to design the LTI filter $\mathcal{C}_\Delta(s)$ in Fig. 4 as

$$\mathcal{C}_\Delta(s) = \Delta_{\mathcal{C}_2}^{-1}(s)\Delta_{\mathcal{C}_1}(s). \tag{7}$$

Design criterion 1. The LTI controllers $\mathcal{C}_i(s)$, $i = 1,2$, are designed such that they do not contain non-minimum phase zeros and have an equal relative degree, although their state dimensions may vary. The filter $\mathcal{H}(s)$ is designed such that no pole-zero cancelations take place in (6), and as a result, in (7).

Note that by Design criterion 1, $\mathcal{C}_\Delta(s)$ as in (7) is a proper filter because its relative degree is zero. This follows from the fact that $\mathcal{C}_i(s)$, $i = 1,2$, have an equal relative degree and, consequently, so do $\Delta_{\mathcal{C}_i}(s)$, $i = 1,2$.

Remark 3. The series connection $\mathcal{C}_2(s)\mathcal{C}_\Delta(s) = \mathcal{C}_1(s)$ has pole-zero cancelations if $\mathcal{C}_2(s) \neq \mathcal{H}(s)$, i.e., the poles/zeros of $\Delta_{\mathcal{C}_2}(s)$ are canceled. However, by Design criterion 1, $\Delta_{\mathcal{C}_2}^{-1}(s)\Delta_{\mathcal{C}_2}(s)$ involves no unstable pole-zero cancelations, i.e., the filter $\Delta_{\mathcal{C}_2}(s)$ does not contain any unstable poles, nor non-minimum phase zeros.

The proposed controller structure in Fig. 4 has all the shared controller dynamics $\mathcal{H}(s)$ active irrespective of the value of the switching function $\alpha(\theta)$, which is advantageous for bumpless transfer and integrator windup, see Zaccarian and Teel (2002). Moreover, by designing $\alpha(\theta) = 0$ when $\theta \notin \Lambda_2$, we have that $\beta(\theta) = 1$ if $\alpha(\theta) \neq 0$, and thus

$$e_{\mathcal{C}_2}(t) = \alpha(\theta(t))\,(r(t) - y_{\mathcal{P}_2}(t)) + (1 - \alpha(\theta(t)))u_{\mathcal{C}_\Delta}(t). \tag{8}$$

As a result, the closed-loop system of Fig. 4 can be treated as a feedback connection between an LTI system and a (to be designed) variable gain $\alpha : \theta \to [0,1]$, and hence belongs to the class of Lur'e-type systems, see e.g., Khalil (2000). The linear dynamical part of the Lur'e-type system description of the closed-loop system is given by

$$\mathcal{G}(s) = \frac{\mathcal{P}_2(s)\mathcal{C}_2(s) - \mathcal{P}_1(s)\mathcal{C}_1(s)}{1 + \mathcal{P}_1(s)\mathcal{C}_1(s)}, \tag{9}$$

denoting the transfer function between 'input' w and 'output' ζ, in feedback with a variable gain element $\alpha : \theta \to [0,1]$. A realization of the closed-loop dynamics in state-space form can be obtained by collecting the individual state-space models of Σ_{sw} as in (1), $\mathcal{C}_\Delta$ and $\mathcal{C}_2$ in one overall model given as follows

$$\dot{x} = Ax + Bw + Fv \tag{10a}$$
$$\zeta = Cx + D_v v \tag{10b}$$
$$w = -\alpha(\theta)\zeta \tag{10c}$$

with $x \in \mathbb{R}^n$ and external inputs $v = [r \;\; d]^\top \in \mathbb{R}^{n_v}$. The state-space model (10) can be a non-minimal realization for the transfer function (9) due to possible pole-zero cancelations, see Remark 3.

4. STABILITY ANALYSIS

In this section, we present graphical data-based conditions to verify input-to-state stability (ISS) of (10), see Sontag and Wang (1995), of the closed-loop system as in Fig. 4 for every $\alpha : \theta \to [0, 1]$ independent of how $\alpha(\theta(t))$ depends on time $t \in \mathbb{R}_{\geq 0}$. But first, we want to emphasize that the system matrix A of the system (10) is Hurwitz by proper controller design.

Proposition 4. For the motion systems that we consider in this paper, the system matrix A of the system (10) is Hurwitz under the following conditions:

(i) The open-loop $\mathcal{O}_1(j\omega) = \mathcal{P}_1(j\omega)\mathcal{C}_1(j\omega)$ satisfies the Nyquist stability criterion, see Skogestad and Postlethwaite (2005), for all $\omega \in \mathbb{R}$;
(ii) Design criterion 1 holds;
(iii) The controller $\mathcal{C}_1(s)$ does not cancel any unstable dynamics (if present) in $\mathcal{P}_1(s)$, i.e., $\mathcal{P}_1(s)\mathcal{C}_1(s)$ has no unstable pole-zero cancelation.

Proof: The proof is omitted due to page limitations, but can be found in van der Weijst et al. (2016). □

The following theorem poses sufficient conditions under which global exponential stability (GES) of the equilibrium $x^* = 0$ is guaranteed for zero inputs. Moreover, the same conditions guarantee that the system (10) is ISS with respect to r and d. See Sontag and Wang (1995) for the exact definition of ISS.

Theorem 5. Consider the system (10) with variable gain $\alpha : \theta \to [0, 1]$, $t \in \mathbb{R}_{\geq 0}$. Suppose that

(I) The system matrix A is Hurwitz;
(II) There exists a constant $\rho > 1$ such that the transfer function $\mathcal{G}(j\omega)$ satisfies

$$\tfrac{1}{\rho} + Re(\mathcal{G}(j\infty)) > 0 \tag{11}$$

and

$$\tfrac{1}{\rho} + Re(\mathcal{G}(j\omega)) > 0 \quad \text{for all} \;\; \omega \in \mathbb{R}. \tag{12}$$

Then the equilibrium point $x^* = 0$ of the system (10) is GES (when $r = 0$ and $d = 0$), and the system (10) is ISS with respect to r and d.

Proof: The proof is omitted due to page limitations, but can be found in van der Weijst et al. (2016). □

Theorem 5 is based on the circle criterion, see e.g., Khalil (2000), which offers data-based graphical frequency-domain conditions to assess closed-loop stability of systems of the form (10), see e.g., Heertjes et al. (2009). The circle criterion in its standard form, see Khalil (2000), requires minimality of the system (10). However, due to our proposed controller structure minimality of the system (10) is lost, see Remark 3. Nevertheless, under the mild

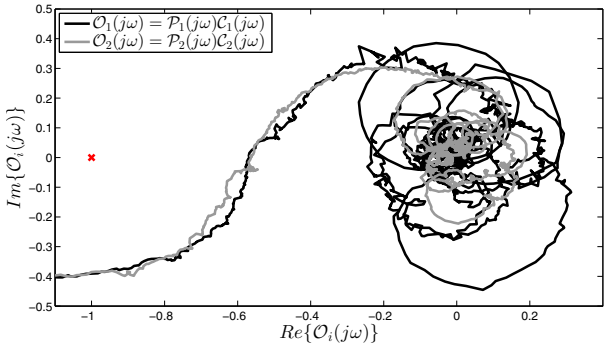

Fig. 5. Nyquist diagrams of the open loops $\mathcal{O}_i(j\omega) = \mathcal{P}_i(j\omega)\mathcal{C}_i(j\omega)$, $i = 1, 2$.

Design criterion 1, we obtain that A is Hurwitz (according to Proposition 4), which together with the circle criterion condition in (II) leads to GES and ISS even though the minimality condition is not satisfied.

5. EXPERIMENTAL RESULTS ON A WAFER STAGE

5.1 Design of the proposed scheduled controller

The scheduled controller is *exactly* implemented as represented in the block-scheme given in Fig. 4, in which the switching of $\alpha : \theta \to [0, 1]$ is currently implemented by a discontinuous switch given by

$$\alpha(\theta) = \begin{cases} 1 & \text{when } \theta \in \Lambda_2 \\ 0 & \text{when } \theta \notin \Lambda_2. \end{cases} \tag{13}$$

The LTI controllers $\mathcal{C}_i(s)$, $i = 1, 2$, are loop-shaped based on the corresponding plant FRFs $\mathcal{P}_i(j\omega)$, $i = 1, 2$, see Fig. 3. Both controllers consist of a PID filter, a second-order low pass filter, and a limited number of notch filters. In this case study, the structure of both controllers is almost identical except for one additional notch filter in $\mathcal{C}_1(s)$, necessary to compensate for the structural mode around ± 1150 Hz in $\mathcal{P}_1(j\omega)$, see Fig. 3. Without the phase lag introduced by this notch filter, $\mathcal{C}_2(s)$ can have a higher gain for frequencies below the bandwidth, thereby increasing the tracking performance. Stability of each *individual/local* closed loop is verified by means of the Nyquist criterion, see Skogestad and Postlethwaite (2005) and Fig. 5, which shows robust stability given a modulus margin of approximately 8 dB. Consequently, the conditions of Proposition 4 are met, thereby satisfying condition (I) of Theorem 5. The final step in the design is to verify the circle criterion condition (II) in Theorem 5. Let us first note that condition (11) is trivial for many motion systems, since $\mathcal{G}(j\omega) \to 0$ for $\omega \to \infty$. The second condition (12) is verified by means of Fig. 6, which represents the Nyquist diagram of $\mathcal{G}(j\omega)$ as in (9), showing that $Re(\mathcal{G}(j\omega)) > -\frac{1}{\rho}$, for some $\rho > 1$ is met [1] for all $\omega \in \mathbb{R}$.

5.2 Experimental results

In this section, the proposed scheduled controller approach is applied to control the z-axis of the motion stage as introduced in Section 2.1. Moreover, we compare the obtained results with those using a SISO LTI controller

[1] The user can influence $Re(\mathcal{G}(j\omega))$ by means of the design of $\mathcal{C}_i(s)$, $i = 1, 2$, and thus the circle criterion condition (II).

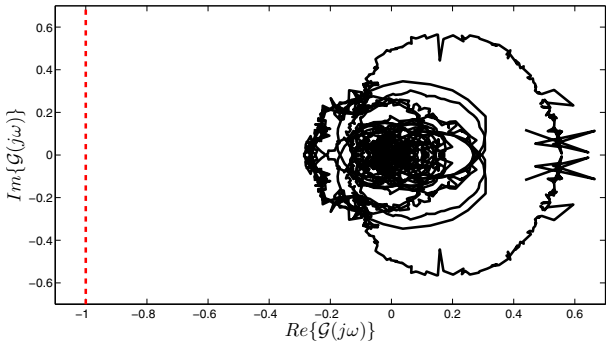

Fig. 6. Nyquist diagram of $\mathcal{G}(j\omega)$ as in (9).

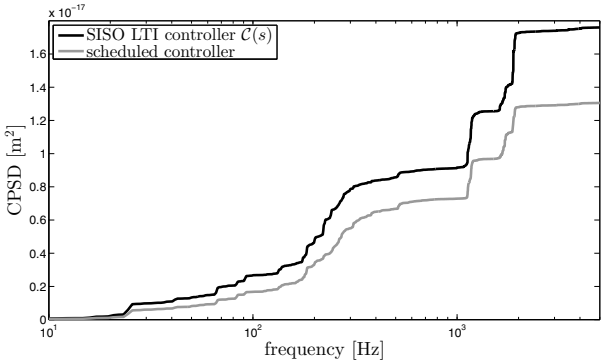

Fig. 7. CPSD of z-axis tracking error.

$\mathcal{C}(s)$ as described in Section 2.3, which is selected as $\mathcal{C}(s) = \mathcal{C}_1(s)$. The setpoint used during the experiments consists of a trajectory in y-direction, depicted schematically in the (x, y)-plane by the red line in Fig. 2(b). Fig. 7 shows the cumulative power spectral density (CPSD) of the tracking error response of the z-axis for both control strategies, which shows a performance increase over the complete frequency range. Intuitively, this can be explained as follows. For frequencies below the closed-loop bandwidth ($\pm$300 Hz), this is a result of the higher feedback gain of $\mathcal{C}_2(s)$. For frequencies above the bandwidth, this is due to the absence of two structural modes that appear in $\mathcal{P}_1(j\omega)$, at $\pm$1150 Hz and at $\pm$1900 Hz, which do not appear in $\mathcal{P}_2(j\omega)$, see Fig. 3.

6. CONCLUSIONS

In this paper, we proposed a novel scheduling control architecture for dynamical systems with position-dependent switching sensor configurations in the context of an industrial wafer stage. Based on the actual measured position of the motion system, dedicated (local) linear time-invariant (LTI) controllers are switched on or off. To meet the requirements from industry, we present a design methodology using classical frequency-domain loop-shaping techniques based on measured frequency response functions (FRFs), and we chose an architecture that is implementable in a standard software environment. Moreover, easy-to-handle data-based conditions are presented that allow the user to verify whether the scheduled feedback control system is input-to-state stable with respect to external disturbances, measurement noise and reference signals, irrespective of how the switching between the controllers occurs in time. In fact, these frequency-domain conditions are based on a generalized form of the circle criterion for which minimality of the underlying system is not required. The practical feasibility of the proposed controller scheduling architecture, as well as the ability to outperform the state-of-the-art industrial control solution, has been experimentally demonstrated on an industrial wafer stage system.

REFERENCES

Butler, H. (2011). Position control in lithographic equipment. *Contr. Syst. Mag.*, 31(5), 28–47.

Deaecto, G.S., Geromel, J.C., and Daafouz, J. (2011). Dynamic output feedback H_∞ control of switched linear systems. *Automatica*, 47(8), 1713 – 1720.

Groot Wassink, M., van de Wal, M., Scherer, C., and Bosgra, O.H. (2005). LPV control for a wafer stage: Beyond the theoretical solution. *Contr. Engineering Practice*, 13(2), 231–245.

Heemels, W.P.M.H., De Schutter, B., Lunze, J., and Lazar, M. (2010). Stability analysis and controller synthesis for hybrid dynamical systems. *Phil. Trans. R. Soc. A*, 368(1930), 4937–4960.

Heertjes, M.F., Schuurbiers, X.G.P., and Nijmeijer, H. (2009). Performance-improved design of N-PID controlled motion systems with applications to wafer stages. *IEEE Trans. Indus. Electronics*, 56(5), 1347–1355.

Khalil, H.K. (2000). *Nonlinear Systems*. Prentice Hall.

Leith, D.J. and Leithead, W.E. (2000). Survey of gain-scheduling analysis and design. *Int. J. of Control*, 73(11), 1001–1025.

Liberzon, D. (2003). *Switching in systems and control*. Birkhauser.

Rugh, W.J. and Shamma, J.S. (2000). Research on gain scheduling. *Automatica*, 36(10), 1401–1425.

Scherer, C.W. (2001). LPV control and full block multipliers. *Automatica*, 37(3), 361–375.

Seron, M.M., Braslavsky, J.H., and Goodwin, G.C. (1997). *Fundamental Limitations in Filtering and Control*. Berlin: Springer.

Shamma, J.S. and Athans, M. (1991). Guaranteed properties of gain scheduled control for linear parameter-varying plants. *Automatica*, 27(3), 559–564.

Skogestad, S. and Postlethwaite, I. (2005). *Multivariable Feedback Control: Analysis and Design*. John Wiley & sons, Ltd.

Sontag, E.D. and Wang, Y. (1995). On characterizations of the input-to-state stability property. *Syst. Control Lett.*, 24(5), 351–359.

Steinbuch, M. and Norg, M.L. (1998). Advanced motion control: An industrial perspective. *European J. of Control*, 4(4), 278–293.

van de Wal, M., van Baars, G., Sperling, F., and Bosgra, O.H. (2002). Multivariable $\mathcal{H}_\infty/\mu$ feedback control design for high-precision wafer stage motion. *Contr. Engineering Practice*, 10, 739–755.

van der Weijst, R., van Loon, S.J.L.M., Heertjes, M.F., and Heemels, W.P.M.H. (2016). Scheduled controller design for systems with varying sensor configurations: A frequency-domain approach. *in preparation*.

Zaccarian, L. and Teel, A.R. (2002). A common framework for anti-windup, bumpless transfer and reliable designs. *Automatica*, 38(10), 1735 – 1744.